Intra-mitochondrial Methylation Deficiency Due to Mutations in *SLC25A26*

Yoshihito Kishita,[1,16] Aleksandra Pajak,[2,16] Nikhita Ajit Bolar,[3,16] Carlo M.T. Marobbio,[4,16] Camilla Maffezzini,[2] Daniela V. Miniero,[4] Magnus Monné,[4,5] Masakazu Kohda,[6] Henrik Stranneheim,[7,8] Kei Murayama,[9] Karin Naess,[7,10] Nicole Lesko,[7,10] Helene Bruhn,[7,10] Arnaud Mourier,[11] Rolf Wibom,[7,10] Inger Nennesmo,[12] Ann Jespers,[13] Paul Govaert,[13] Akira Ohtake,[14] Lut Van Laer,[3] Bart L. Loeys,[3,15] Christoph Freyer,[2,7] Ferdinando Palmieri,[4,17,*] Anna Wredenberg,[2,7,17,*] Yasushi Okazaki,[1,6,17] and Anna Wedell[2,7,8,17]

S-adenosylmethionine (SAM) is the predominant methyl group donor and has a large spectrum of target substrates. As such, it is essential for nearly all biological methylation reactions. SAM is synthesized by methionine adenosyltransferase from methionine and ATP in the cytoplasm and subsequently distributed throughout the different cellular compartments, including mitochondria, where methylation is mostly required for nucleic-acid modifications and respiratory-chain function. We report a syndrome in three families affected by reduced intra-mitochondrial methylation caused by recessive mutations in the gene encoding the only known mitochondrial SAM transporter, SLC25A26. Clinical findings ranged from neonatal mortality resulting from respiratory insufficiency and hydrops to childhood acute episodes of cardiopulmonary failure and slowly progressive muscle weakness. We show that *SLC25A26* mutations cause various mitochondrial defects, including those affecting RNA stability, protein modification, mitochondrial translation, and the biosynthesis of CoQ10 and lipoic acid.

Altered S-adenosylmethionine (SAM) concentrations in the cytoplasm have been suggested to be involved in the pathophysiology of disease and in the natural aging process.[1,2] Highly specialized methyltransferases, encoding approximately 1%–2% of eukaryotic genomes,[3] use SAM as a methyl group donor to methylate their targets. The human mitochondrial SAM carrier (SAMC), encoded by *SLC25A26* (MIM: 611037), is expressed in all human tissues examined and is believed to be the only route of SAM entry into mitochondria.[4] However, regulatory mechanisms of intra-mitochondrial SAM (mtSAM) concentrations or other pathways modulating mtSAM levels are unknown, and so far the pathophysiological consequences of reduced mitochondrial SAM import are unclear.

We identified three families with different ethnic origins and a complex biochemical phenotype caused by mutations in *SLC25A26*. Individual 1 (P1, individual II:2 from family 1 in Figure 1A) was born to consanguineous parents from Iraq and presented at 4 weeks with acute circulatory collapse and pulmonary hypertension, requiring extra-corporeal membrane oxygenation for 5 days. He had severe lactic acidosis around 20 mmol/l (reference: 0.5–2.3). Sodium dichloroacetic acid had good effect, and the boy slowly normalized. At 3.5 years, he had a second episode of pulmonary hypertension, which also normalized. At 6 years 3 months, the boy had increasing muscle weakness, fatigue, recurrent abdominal pain, lack of appetite, and slightly delayed development. Investigation of mitochondrial function from a muscle biopsy revealed reduced activities of complexes I and IV and a reduced ATP production rate, in particular when pyruvate was used as a substrate (Figures S1A and S1B). Histology showed the presence of COX-negative muscle fibers (Figure S1C). Additionally, Blue-native PAGE (BN-PAGE) revealed reduced levels of assembled complexes I and IV (Figure S1D). Individual 2 (P2, II:1 from family 2 in Figure 1A), born to Japanese parents, developed severe lactic acidosis up to 42 mmol/l (reference: <1.8), an elevated pyruvate level (0.65 mmol/l; reference: <0.1), and respiratory failure 11 hr after birth, prompting mechanical

[1]Division of Functional Genomics & Systems Medicine, Research Center for Genomic Medicine, Saitama Medical University, 1397-1 Yamane, Hidaka-shi, Saitama 350-1241, Japan; [2]Max Planck Institute Biology of Ageing – Karolinska Institutet Laboratory, Division of Metabolic Diseases, Department of Laboratory Medicine, Karolinska Institutet, 171 77 Stockholm, Sweden; [3]Department of Medical Genetics, Faculty of Medicine and Health Sciences, Antwerp University Hospital, University of Antwerp, Antwerp 2650, Belgium; [4]Department of Biosciences, Biotechnologies and Biopharmaceutics, University of Bari, Via Edoardo Orabona 4, 70125 Bari, Italy; [5]Department of Sciences, University of Basilicata, Via Ateneo Lucano 10, 85100 Potenza, Italy; [6]Division of Translational Research, Research Center for Genomic Medicine, Saitama Medical University, 1397-1 Yamane, Hidaka-shi, Saitama 350-1241, Japan; [7]Centre for Inherited Metabolic Diseases, Karolinska University Hospital, 171 76 Stockholm, Sweden; [8]Science for Life Laboratory and Department of Molecular Medicine and Surgery, Karolinska Institutet, 171 76 Stockholm, Sweden; [9]Department of Metabolism, Chiba Children's Hospital, 579-1 Heta-cho, Midori, Chiba 266-0007, Japan; [10]Department of Laboratory Medicine, Karolinska Institutet, 171 77 Stockholm, Sweden; [11]Max Planck Institute for Biology of Ageing, 50931 Cologne, Germany; [12]Department of Pathology, Karolinska University Hospital, 171 77 Stockholm, Sweden; [13]Paola Children's Hospital, ZNA Middelheim, Antwerp 2650, Belgium; [14]Department of Pediatrics, Saitama Medical University, 38 Morohongo Moroyama-machi, Iruma-gun, Saitama 350-0495, Japan; [15]Department of Genetics, Radboud University Medical Center, Nijmegen, 6525 GA, the Netherlands
[16]These authors contributed equally to this work
[17]These authors contributed equally to this work
*Correspondence: ferdinando.palmieri@uniba.it (F.P.), anna.wredenberg@ki.se (A.W.)
http://dx.doi.org/10.1016/j.ajhg.2015.09.013.

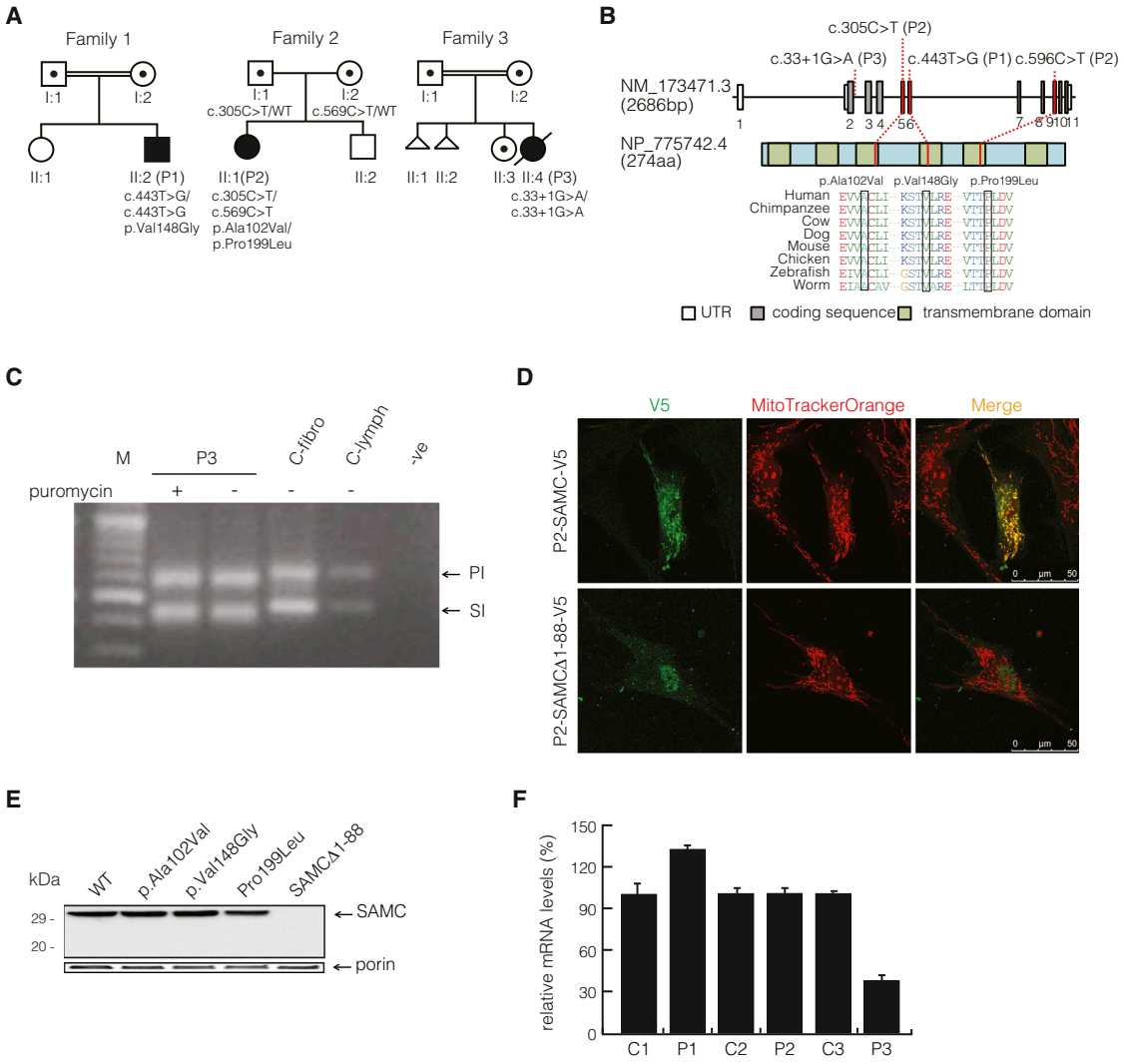

Figure 1. Identification of Mutations in *SLC25A26*

(A) Pedigrees of individuals P1–P3 indicate the inheritance patterns in the individuals' families. P1 was born to consanguineous parents from Iraq after a normal pregnancy and neonatal period. P2 was born full term to unrelated parents from Japan with an Apgar score of 9-10. P3 was born to consanguineous parents of Moroccan descent. Symbols and colors are defined as follows: square, male; circle, female; triangle, miscarriage with unknown gender; white, unaffected; dot, unaffected carrier; black, affected. WT indicates wild-type.

(B) Diagram representing the relative positions of *SLC25A26* mutations (NM_173471.3) and SLC25A26 alterations (GenBank: NP_775742.4). Amino acid alignments of eight species show the regions of each mutation.

(C) *SLC25A26* mutation c.33+1G>A causes an RNA-splicing defect: the top band in lanes 2–5 indicates the amplification of the principal isoform (PI; Ensembl: ENST00000354883), and the lower band in lanes 2–5 indicates the amplification of the shorter isoform (SI; Ensembl: ENST00000336733). As a result of the mutation, PCR products from the individual, treated both with and without puromycin, were observed to be shorter in length (top band: PI around 572 bp; lower band: SI around 415 bp) than those of the control fibroblasts and lymphocytes (top band: PI 617 bp; lower band: SI 450 bp). No difference was observed between the puromycin-treated and non-puromycin-treated P3 samples. Lane contents are as follows: lanes 1 and 7, 100 bp DNA ladder (Fermentas); lane 2, PCR products amplified from cDNA extracted from P3 fibroblasts treated with puromycin; lane 3, PCR products amplified from cDNA extracted from P3 fibroblasts cultured without puromycin; lane 4, PCR products amplified from cDNA extracted from control fibroblasts; lane 5, PCR products amplified from cDNA extracted from control lymphocytes; and lane 6, PCR reaction blank.

(D) Subcellular localization of C-terminal V5-tagged SAMC (p2-SAMC-V5) and the shortened SAMCΔ1–88 (p2-SAMCΔ-V5) in P2 fibroblasts stained with MitoTrackerOrange.

(E) Amounts of wild-type (WT) SAMC, p.Ala102Val SAMC, p.Val148Gly SAMC, p.Pro199Leu SAMC, SAMCΔ1–88, and endogenous porin in mitochondria from SAM5Δ yeast transformed with WT SAMC-pYES2 (SAMC), p.Ala102Val SAMC-pYES2 (p.Ala102Val), p.Val148Gly SAMC-pYES2 (p.Val148Gly), p.Pro199Leu SAMC-pYES2 (p.Pro199Leu), and short SAMC-pYES2 (SAMCΔ1–88). Equal amounts of mitochondrial lysates (30 μg protein) were separated by SDS-PAGE, transferred to nitrocellulose, and immunodecorated with the anti-hemagglutinin or the anti-porin antibody.

(F) Relative *SLC25A26* mRNA steady-state levels in fibroblasts as determined by qRT-PCR. Values are normalized to 18S rRNA levels. Error bars show the SEM.

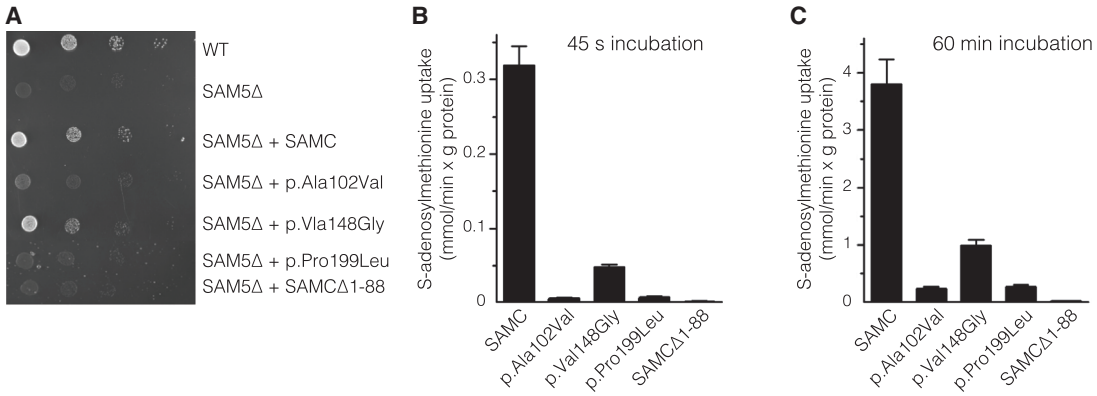

Figure 2. In Vivo and In Vitro Pathology of the *SLC25A26* Mutations
(A) 4-fold serial dilution of wild-type (WT) yeast cells, SAM5Δ cells, and SAM5Δ cells transformed with WT SAMC-pYES2 (SAMC), p.Ala102Val SAMC-pYES2 (p.Ala102Val), p.Val148Gly SAMC-pYES2 (p.Val148Gly), p.Pro199Leu SAMC-pYES2 (p.Pro199Leu), and short SAMC-pYES2 (SAMCΔ1–88) were plated on YP medium supplemented with 3% glycerol and 0.05% galactose for 72 hr at 30°C.
(B and C) Liposomes reconstituted with WT or the indicated SAMC variants were preloaded with 10 mM S-adenosylmethionine at 25°C. Transport was started with 1 mM [^{3}H]S-adenosylmethionine and terminated after (B) 45 s or (C) 60 min. The values are means ± SD of at least four independent experiments.

ventilation and dichloroacetic acid treatment. The child improved, and gross development was normal until 2 years of age, when she experienced an additional episode of severe lactic acidosis (36 mmol/l) followed by cardiopulmonary arrest and hypoxic brain damage. After this episode, the individual has remained severely handicapped. Activities of respiratory-chain enzymes were normal in fibroblasts but showed decreased activities of complexes I, III, and IV in skeletal muscle (Figure S1E). Muscle histology was normal at day 6 but revealed both ragged red fibers and COX-negative fibers when individual 2 was 3 years of age (Figure S1F). Individual 3 (P3, individual II:4 from family 3 in Figure 1A), born to consanguineous parents of Moroccan decent, was delivered by caesarean section at 30 weeks 5 days after reduced fetal movements, polyhydramnios, fetal hydrops, and poor cardiotocography (CTG) readings were noted from 27 weeks of gestational age. She had normal antropometric parameters (birth weight 1,300 g, length 38 cm, and head circumference 27.5 cm) but presented with a poor Apgar score (3-5-6) due to bradycardia, hypotonia, and respiratory insufficiency, necessitating assisted ventilation with high-frequency oscillation. Urine lactate and pyruvate levels were 18 mmol/mmol creatinine (reference: 1–285 μmol/mmol creatinine) and 1.2 mmol/mmol creatinine (reference: 1–130 μmol/mmol creatinine), respectively. Brain ultrasound demonstrated cystic necrosis of the germinal matrix (extensive symmetrical caudothalamic germinolysis) and mild striatal arteriopathy. The child died of respiratory and multiple organ failure at 5 days of age. Measurement of respiratory-chain activity in fibroblasts demonstrated decreased complex IV activity. Additional clinical descriptions and experimental details are provided in the Supplemental Note.

Written informed consent was obtained from the parents, and investigations were performed according to the regional ethics committees at the Karolinska Institutet (Sweden), the Saitama Medical University (Japan), and Antwerp University Hospital (Belgium).

Homozygosity mapping, exome sequencing,[5–11] and Sanger confirmation (Figures 1A and 1B and Figure S2A) revealed *SLC25A26* mutations (GenBank: NM_173471.3) in all affected individuals and their parents. We identified conserved missense mutations in P1, homozygous for a c.443T>C (p.Val148Gly) substitution, and P2, compound heterozygous for c.305C>T (p.Ala102Val) and c.596C>T (p.Pro199Leu). P3 was homozygous for a splice mutation (c.33+1G>A) (Figure 1C), which results in either a frameshift mutation in *SLC25A26*, when an alternative splice site in exon 2 is used, or a shorter polypeptide lacking the first 88 amino acids (SAMCΔ1–88), as a result of an alternative translation initiation site in exon 4 (Figure S2B). Cloning and sequencing of cDNA from P3 fibroblasts of this region confirmed the presence of exclusively alternative splice variants (Figure S2C). The shortened transcript lacks the first two transmembrane helices (Figure S3) and failed to co-localize (Figure 1D) or be detected in mitochondria by western blot analysis (Figure 1E), indicating that it does not encode a functional mitochondrial carrier protein. Additionally, the splice mutation resulted in reduced *SLC25A26* mRNA transcript levels in fibroblasts from P3, whereas P1 and P2 samples were unaffected (Figure 1F).

The conservation of all three missense mutations among 87 species (Ala102 [84%], Val148 [100%, including Leu and Ile], and Pro199 [100%]) suggests that their replacement might disrupt protein function. We also considered the transversal scores of the altered SAMC residues (these scores are a measure of the strength of the evolutionary selection acting on the residues) from a study of the rate of single-nucleotide evolution.[12] These values (4.52 for Ala102, 3.68 for Val148, and 5.15 for Pro199) are all close to or greater than 3.7, previously shown to represent sites of functional importance in mitochondrial carriers.[12] Furthermore, the position of all three *SLC25A26* missense mutations in the structural homology model

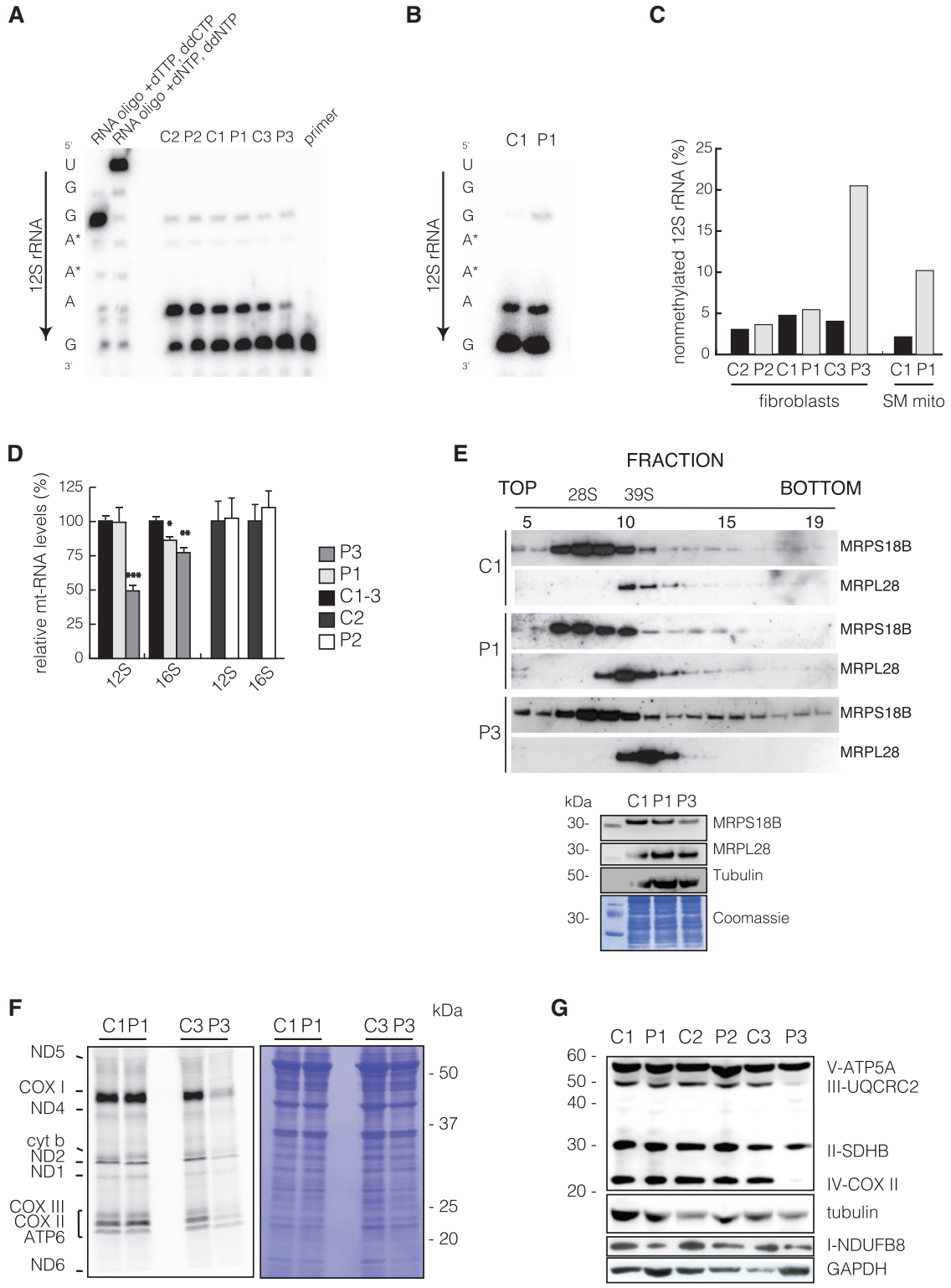

Figure 3. Affected Mitochondrial Translation

(A and B) Poisoned primer extension on total RNA from (A) fibroblasts or (B) skeletal-muscle mitochondria and subsequent size separation by denaturing PAGE. [^{32}P] end-labeled oligo complement to the 3′ terminus of 12S rRNA was annealed to RNA extracts and elongated in the presence of dTTP and ddCTP by M-MLV reverse transcriptase. In the case of adenine dimethylation, reverse transcription will terminate upstream of the dimethylation, whereas in its absence, termination will occur immediately downstream of the first guanidine residue because of ddCTP.

(C) Quantification of termination and read-through of (A) and (B).

(D) qRT-PCR of the steady-state levels of 12S and 16S rRNA in fibroblasts. The mean value of two independent experiments performed in triplicate is shown.

(legend continued on next page)

of SAMC also suggested a pathogenic effect of the mutations (Figure S4).[13] We confirmed pathogenicity by complementation studies in an *S. cerevisiae* SAMC-null strain (SAM5Δ)[14] by revealing that the growth phenotype of SAM5Δ cells on non-fermentable carbon sources could not be restored by complementation of the knockout strain with the p.Ala102Val, p.Pro199Leu, or SAMCΔ1–88 variant. Only the p.Val148Gly altered SAMC partially rescued the growth defect of SAM5Δ cells (Figure 2A). Additionally, we measured SAM transport capacity in reconstituted liposomes as previously described[15–19] and demonstrated a severe abrogation of SAM transport capacity for all altered proteins (Figures 2B and 2C and Figure S5). SAMCΔ1–88 was completely inactive, whereas p.Ala102Val and p.Pro199Leu variants exhibited negligible activity, and p.Val148Gly strongly inhibited SAMC activity (15% of wild-type SAMC). All together, conservation scores, yeast complementation, and in vitro reconstitution studies confirm the deleterious consequences of the *SLC25A26* mutations on SAMC function. Also supporting this is that the various degrees of residual SAM-import capacity correlated well with the severity of the clinical presentation and biochemical phenotype in the affected individuals.

Methylation is required for a multitude of mitochondrial processes, including RNA and protein modifications, and we therefore investigated the status of adenine dimethylation in the hairpin loop at the 3′ end of the mitochondrial 12S rRNA by poisoned primer extension,[20] known to be methylated via mtSAM.[21–23] In control samples, the majority of 12S rRNA molecules were dimethylated at adenines 936–937, whereas fibroblasts from P3 (Figure 3A) and skeletal-muscle mitochondria from P1 (Figure 3B) revealed a substantial shift from methylated to non-methylated ribosomal transcripts (Figure 3C). Surprisingly, not only did we fail to observe a methylation defect in fibroblast samples from individuals P1 and P2, but there was also substantial termination of primer extension in P3 fibroblasts, suggesting some methylation of 12S rRNA despite the complete lack of SAMC activity. 12S rRNA steady-state levels are dependent on adenine dimethylation,[23] and in agreement with this, 12S rRNA steady-state levels in fibroblasts from P3 were decreased (Figure 3D), whereas all other transcripts tested had only mild changes (Figures S6A and S6B). Additionally, mitochondrial ribosomal assembly was only moderately affected in P3, who showed reduced amounts of the small and possible stabilization of the large mitochondrial ribosome subunits (Figure 3E). Despite the mild effect on mitochondrial ribosome assembly, de novo mitochondrial translation[25] was severely affected in P3 fibroblasts (Figure 3F), possibly because methylation is required for tRNA maturation. This defect is also reflected by the reduced steady-state level of COXII (Figure 3G), a subunit of complex IV, and most likely contributes to the mitochondrial dysfunction in P1 skeletal muscle, which showed reduced levels of complexes I and IV (Figure S1).

Several mitochondrial proteins are known to be methylated by S-adenosylmethionine-dependent methyltransferases.[26,27] We studied the methylation status of three known mitochondrial SAM targets, ADP/ATP translocators ANT1 and ANT2, and the electron-transferring flavoprotein ETFB. Western blot analysis against di- and tri-methyl lysine (DTML) revealed decreased methylation levels in all fibroblast samples from affected individuals, and P3 was the most severely affected (Figure 4A). Transfection of cell lines from affected individuals with exogenous ANT1 and ANT2 further confirmed the methylation deficiency (Figure 4B). Loss of protein methylation was further rescued by wild-type SAMC in fibroblasts from P2 and P3 (Figure 4C).

Lipoic acid (LA) metabolism depends heavily on SAM-dependent methylation within mitochondria.[31] Individual P1 presented with high plasma glycine and low ATP production in muscle when pyruvate was used as a substrate, consistent with deficiencies of the glycine cleavage system and the pyruvate dehydrogenase complex, both of which require LA. These measurements were not performed for individual P2 or P3. Fibroblasts from individuals P1–P3 showed reduced levels of the LA subunits pyruvate dehydrogenase complex E2 (PDHC-E2) and alpha-ketoglutarate dehydrogenase E2 (α-KGDH-E2) (Figures 4D and 4E), and P3 was the most severely affected. This decrease was not secondary to the mitochondrial dysfunction observed, given that two independent samples from individuals with unrelated mitochondrial diseases showed normal levels of LA (M1 and M2 in Figure 4E), whereas samples from individuals with mutations affecting LA biosynthesis were severely reduced (B1–B4 in Figure 4E).

The final steps of coenzyme Q_{10} (CoQ_{10}) biosynthesis, including several methylation steps of the benzoquinone ring, are performed within the mitochondrial network.[32] We therefore measured CoQ_{10} levels in isolated skeletal-muscle mitochondria from P1 as previously described[7,28] and observed that they were severely decreased, presumably as a result of impaired CoQ_{10} biosynthesis (Figure 4F). In order to investigate the bioenergetic

(E) Ribosomal gradients (top panel) from fibroblast mitochondria of P1 and P3. Ribosomes were separated in 10%–30% sucrose gradient by centrifugation and then fractionated as previously described,[24] with slight modifications. Western blot analysis against subunits of the small ribosomal subunit (28S; MRPS18B) or large subunit (39S; MRPL28) revealed their individual migration and ribosomal monosome (55S) formation. Loading onto the gradient was controlled by input western blot analysis (bottom panel) against mtSSU (MRPS18B), mt-LSU (MRPL28), and tubulin. Additionally, a Coomassie stain is shown.
(F) For determining de novo translation,[25] fibroblasts were cultured for 45 min in the presence of [^{35}S] methionine and cysteine; then, protein extracts were separated by SDS-PAGE, and the gel was exposed. The low-molecular-weight subunits of ND3, ATP8, and ND4L are not shown.
(G) Western blot analysis of fibroblasts used antibodies against nuclear-encoded subunits of complexes I–V.

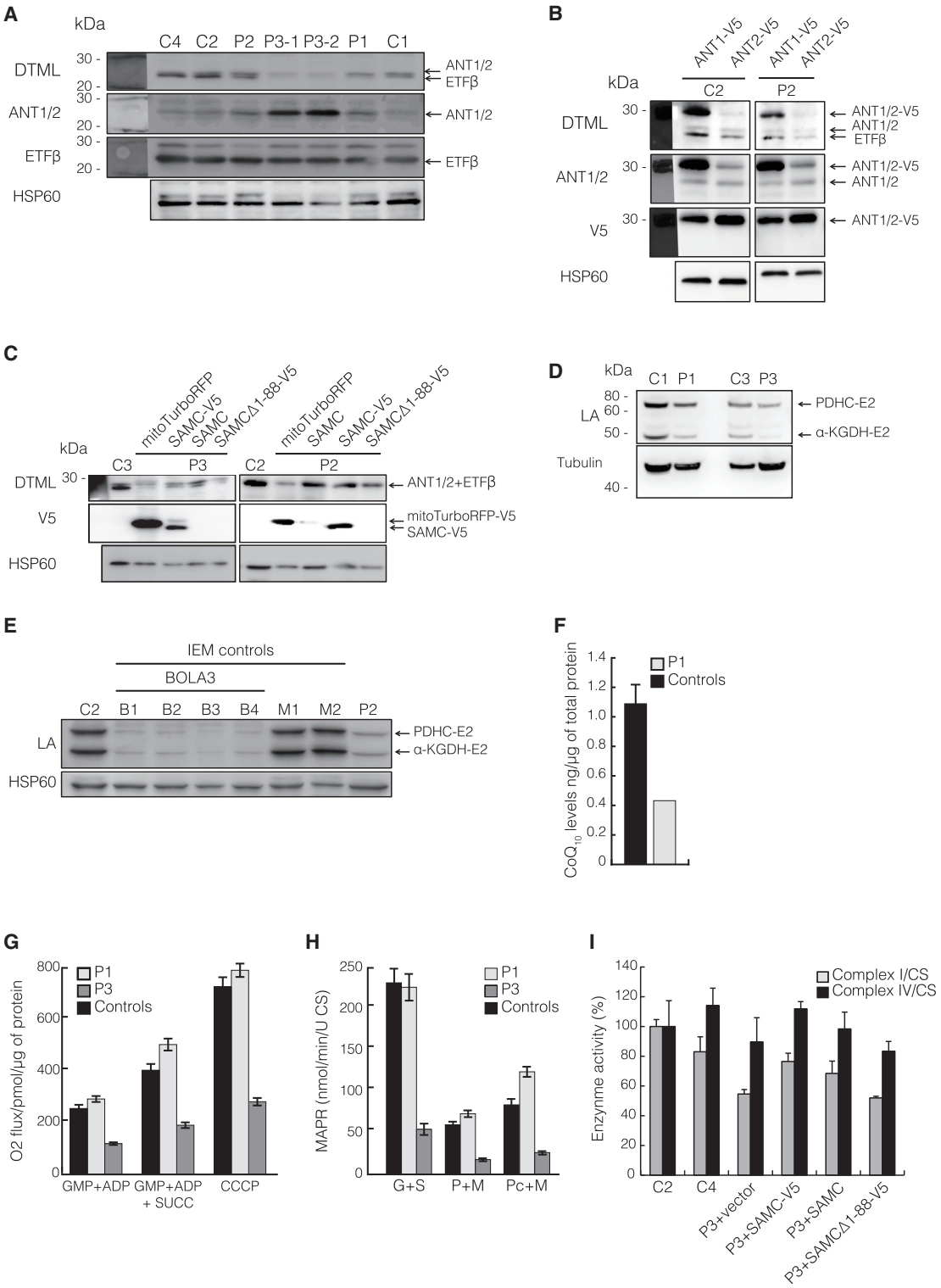

Figure 4. Effects of Reduced Mitochondrial Methylation

(A) Steady-state levels of ANT1, ANT2, and ETFβ (middle panels) in individuals P1–P3 and control cells (C1, C2, and C4), as well as DTML levels (upper panel) normalized to HSP60.

(B) Control (C2) or P2 fibroblasts were transfected with V5-tagged isoforms of ANT (ANT1-V5 and ANT2-V5) for determining DTML methylation of ANT1-V5 and ANT2-V5.

(C) Western blot analysis of DTML levels in samples from control (C2 and C3) and P2 and P3 fibroblasts transfected with empty vector (mitoTurboRFP), wild-type SAMC (SAMC), V5-tagged SAMC (SAMC-V5), or the N-terminal-truncated SAMC (SAMCΔ-V5).

(D and E) Western blot analysis of the lipoic acid (LA) subunits pyruvate dehydrogenase complex E2 (PDHC-E2) and alpha-ketoglutarate dehydrogenase E2 (α-KGDH-E2) in (D) control (C1 and C3) and P1 and P3 samples or in (E) control (C2) or affected (B1–B4, M1 and M2,

(legend continued on next page)

consequences of reduced mtSAM import, we measured both oxygen consumption (Figure 4G) and mitochondrial ATP production rates (Figure 4H) in fibroblasts carrying the mildest (P1) or null (P3) mutations. Fibroblasts from P3 showed reduced oxygen consumption (Figure 4G) and reduced mitochondrial ATP production rates (Figure 4H), whereas P1 fibroblasts, in contrast to muscle samples (Figure S1A), showed no defect. Finally, the biochemical defects of P3 fibroblasts in the activity of complexes I and IV was rescued by transiently expressing wild-type and tagged wild-type SAMC, but not SAMCΔ1–88 (Figure 4I).

In summary, we have presented three individuals affected by a primary defect in the mitochondrial methylome. Our results show that impaired SAM transport into mitochondria causes a complex syndrome causing multiple primary defects, including those affecting RNA stability, protein modification, mitochondrial translation, and the biosynthesis of CoQ_{10} and LA. We identified three individuals who originate from different ethnic groups and share striking similarities both biochemically and clinically, consistent with the degree of residual SAM-import capacity. Surprisingly, even though we studied SAMC-null samples, we detected some degree of intra-mitochondrial methylation, suggesting that other forms of methylation or recycling of methyl groups originating from imported methylated proteins might occur within mitochondria.

Supplemental Data

Supplemental Data include a Supplemental Note and six figures and can be found with this article online at http://dx.doi.org/10.1016/j.ajhg.2015.09.013.

Acknowledgments

We thank the families who participated in this study; Y. Mogami, K. Tominaga, Y. Tokuzawa, H. Nyuzuki, Y. Yatsuka, S. Tamaru, C. Shimizu, and S. Suzuki for technical assistance; and H. Miyoshi of Keio University and RIKEN BioResource Center for the CS-CA-MCS plasmid. This work was supported by the Japanese Ministry of Education, Culture, Sports, Science, and Technology (Innovative Cell Biology by Innovative Technology and Strategic Research Centers at private universities) and the Takeda Science Foundation to Y.O.; Japan Society for the Promotion of Science KAKENHI 20634398 to Y.K.; Research on Intractable Diseases (Mitochondrial Disorder) from the Ministry of Health, Labor, and Welfare of Japan to A.O.; and Grants-in-Aid for the Practical Research Project for Rare/Intractable Diseases from the Japan Agency for Medical Research and Development to K.M. Support was also given by the Swedish Research Council (A. Wedell [VR12198]; A. Wredenberg [VR521-2012-2571]); Karolinska Institutet (A. Wredenberg [2013fobi38557]; C.F. [2013fobi37932]); Åke Wiberg Foundation (A. Wredenberg [738762088]; C.F. [367990950]); Stockholm County Council (A. Wedell [20140053]; A. Wredenberg [K0176-2012]); Swedish Foundation for Strategic Research (A. Wredenberg [ICA 12-0017]); and Knut & Alice Wallenberg Foundation (A. Wedell and A. Wredenberg [KAW 20130026]). A. Wredenberg is a Ragnar Söderberg fellow (M77/13). F.P. received grants from the Comitato Telethon Fondazione Onlus (GGP11139) and Italian Human ProteomeNet (RBRNO7BMCT-009). B.L.L. is a senior clinical investigator of the Fund for Scientific Research, Flanders (FWO, Belgium), holds a European Research Council (ERC) starting grant, and received additional support from the FWO (G.0221.12) and ERC.

Received: August 14, 2015
Accepted: September 29, 2015
Published: October 29, 2015

Web Resources

The URLs for data presented herein are as follows:

OMIM, http://www.omim.org
RefSeq, http://www.ncbi.nlm.nih.gov/refseq/

References

1. Carrasco, M., Rabaneda, L.G., Murillo-Carretero, M., Ortega-Martínez, S., Martínez-Chantar, M.L., Woodhoo, A., Luka, Z., Wagner, C., Lu, S.C., Mato, J.M., et al. (2014). Glycine N-methyltransferase expression in the hippocampus and its role in neurogenesis and cognitive performance. Hippocampus *24*, 840–852.
2. Infantino, V., Castegna, A., Iacobazzi, F., Spera, I., Scala, I., Andria, G., and Iacobazzi, V. (2011). Impairment of methyl

and P2) samples. Control samples were obtained from individuals with non-related inborn errors of metabolism (IEMs) and either mutations in *BOLA3* (BolA family member 3) (B1–B4) or unrelated mitochondrial diseases (M1 and M2).
(F) CoQ_{10} levels in mitochondrial extracts from skeletal muscle were determined by ultra-performance liquid chromatography tandem mass spectrometry[7,28] in four control samples (black) and muscles from affected individuals (gray). Control values are the mean ± SD of four control samples.
(G) Mitochondrial oxygen consumption of control (black) or P1 and P3 (gray) fibroblasts. Measurements were performed on an Oroboros oxygraph in the presence of (left) complex I substrates glutamate, malate, pyruvate (GMP), and ADP; (middle) complex I and II substrates GMP, succinate, and ADP; or (right) complex I and II substrates GMP, ADP, succinate, and the mitochondrial uncoupler carbonyl cyanide m-chlorophenyl hydrazone (CCCP). Error bars indicate the SEM of three independent experiments.
(H) Mitochondrial ATP production rate (MAPR)[29] in control (C1–C3; black) and P1 and P3 (gray) fibroblasts was determined by a firefly-luciferase-based method using glutamate and succinate (G+S), pyruvate and malate (P+M), or palmitoyl-L-carnitine and malate (Pc+M) as a substrate at 25°C. Results are presented as the ATP synthesis rate (units) per unit of citrate synthase (CS) activity. Values are the mean ± SEM of three independent experiments.
(I) Isolated enzyme activities[29,30] of complexes I (gray) and IV (black) are normalized to citrate synthase (CS) activities from control (C2 and C4) and P3 fibroblast cell lines after transfection with empty vector (mitoTurboRFP; P3), V5-tagged SAMC (SAMC-V5), SAMC, or V5-tagged SAMCΔ1–88.

cycle affects mitochondrial methyl availability and glutathione levels in Down's syndrome. Mol. Genet. Metab. *102*, 378–382.
3. Clarke, S.G. (2013). Protein methylation at the surface and buried deep: thinking outside the histone box. Trends Biochem. Sci. *38*, 243–252.
4. Agrimi, G., Di Noia, M.A., Marobbio, C.M.T., Fiermonte, G., Lasorsa, F.M., and Palmieri, F. (2004). Identification of the human mitochondrial S-adenosylmethionine transporter: bacterial expression, reconstitution, functional characterization and tissue distribution. Biochem. J. *379*, 183–190.
5. Stranneheim, H. (2014). Mutation Identification Pipeline (MIP), https://github.com/henrikstranneheim/MIP.
6. Stranneheim, H., Engvall, M., Naess, K., Lesko, N., Larsson, P., Dahlberg, M., Andeer, R., Wredenberg, A., Freyer, C., Barbaro, M., et al. (2014). Rapid pulsed whole genome sequencing for comprehensive acute diagnostics of inborn errors of metabolism. BMC Genomics *15*, 1090.
7. Freyer, C., Stranneheim, H., Naess, K., Mourier, A., Felser, A., Maffezzini, C., Lesko, N., Bruhn, H., Engvall, M., Wibom, R., et al. (2015). Rescue of primary ubiquinone deficiency due to a novel COQ7 defect using 2,4-dihydroxybensoic acid. J. Med. Genet. Published online June 17, 2015. http://dx.doi.org/10.1136/jmedgenet-2015-102986.
8. Ohtake, A., Murayama, K., Mori, M., Harashima, H., Yamazaki, T., Tamaru, S., Yamashita, Y., Kishita, Y., Nakachi, Y., Kohda, M., et al. (2014). Diagnosis and molecular basis of mitochondrial respiratory chain disorders: exome sequencing for disease gene identification. Biochim. Biophys. Acta *1840*, 1355–1359.
9. Haack, T.B., Jackson, C.B., Murayama, K., Kremer, L.S., Schaller, A., Kotzaeridou, U., de Vries, M.C., Schottmann, G., Santra, S., Büchner, B., et al. (2015). Deficiency of ECHS1 causes mitochondrial encephalopathy with cardiac involvement. Ann. Clin. Transl. Neurol. *2*, 492–509.
10. Scharpf, R.B., Parmigiani, G., Pevsner, J., and Ruczinski, I. (2008). Hidden Markov models for the assessment of chromosomal alterations using high-throughput SNP arrays. Ann. Appl. Stat. *2*, 687–713.
11. Vandeweyer, G., Reyniers, E., Wuyts, W., Rooms, L., and Kooy, R.F. (2011). CNV-WebStore: online CNV analysis, storage and interpretation. BMC Bioinformatics *12*, 4.
12. Pierri, C.L., Palmieri, F., and De Grassi, A. (2014). Single-nucleotide evolution quantifies the importance of each site along the structure of mitochondrial carriers. Cell. Mol. Life Sci. *71*, 349–364.
13. Palmieri, F. (2013). The mitochondrial transporter family SLC25: identification, properties and physiopathology. Mol. Aspects Med. *34*, 465–484.
14. Marobbio, C.M.T., Agrimi, G., Lasorsa, F.M., and Palmieri, F. (2003). Identification and functional reconstitution of yeast mitochondrial carrier for S-adenosylmethionine. EMBO J. *22*, 5975–5982.
15. Palmieri, F., Indiveri, C., Bisaccia, F., and Iacobazzi, V. (1995). Mitochondrial metabolite carrier proteins: purification, reconstitution, and transport studies. Methods Enzymol. *260*, 349–369.
16. Capobianco, L., Bisaccia, F., Mazzeo, M., and Palmieri, F. (1996). The mitochondrial oxoglutarate carrier: sulfhydryl reagents bind to cysteine-184, and this interaction is enhanced by substrate binding. Biochemistry *35*, 8974–8980.
17. Palmieri, L., De Marco, V., Iacobazzi, V., Palmieri, F., Runswick, M.J., and Walker, J.E. (1997). Identification of the yeast ARG-11 gene as a mitochondrial ornithine carrier involved in arginine biosynthesis. FEBS Lett. *410*, 447–451.
18. Palmieri, L., Arrigoni, R., Blanco, E., Carrari, F., Zanor, M.I., Studart-Guimaraes, C., Fernie, A.R., and Palmieri, F. (2006). Molecular identification of an Arabidopsis S-adenosylmethionine transporter. Analysis of organ distribution, bacterial expression, reconstitution into liposomes, and functional characterization. Plant Physiol. *142*, 855–865.
19. Palmieri, F., and Klingenberg, M. (1979). Direct methods for measuring metabolite transport and distribution in mitochondria. Methods Enzymol. *56*, 279–301.
20. Rio, D.C., Ares, M., Hannon, G.J., and Nilsen, T.W. (2011). RNA: A Laboratory Manual (Cold Spring Harbor Laboratory Press).
21. Helser, T.L., Davies, J.E., and Dahlberg, J.E. (1971). Change in methylation of 16S ribosomal RNA associated with mutation to kasugamycin resistance in Escherichia coli. Nat. New Biol. *233*, 12–14.
22. Poldermans, B., Van Buul, C.P., and Van Knippenberg, P.H. (1979). Studies on the function of two adjacent N6,N6-dimethyladenosines near the 3′ end of 16 S ribosomal RNA of Escherichia coli. II. The effect of the absence of the methyl groups on initiation of protein biosynthesis. J. Biol. Chem. *254*, 9090–9093.
23. Metodiev, M.D., Lesko, N., Park, C.B., Cámara, Y., Shi, Y., Wibom, R., Hultenby, K., Gustafsson, C.M., and Larsson, N.-G. (2009). Methylation of 12S rRNA is necessary for in vivo stability of the small subunit of the mammalian mitochondrial ribosome. Cell Metab. *9*, 386–397.
24. Rorbach, J., Boesch, P., Gammage, P.A., Nicholls, T.J.J., Pearce, S.F., Patel, D., Hauser, A., Perocchi, F., and Minczuk, M. (2014). MRM2 and MRM3 are involved in biogenesis of the large subunit of the mitochondrial ribosome. Mol. Biol. Cell *25*, 2542–2555.
25. Leary, S.C., and Sasarman, F. (2009). Oxidative phosphorylation: synthesis of mitochondrially encoded proteins and assembly of individual structural subunits into functional holoenzyme complexes. Methods Mol. Biol. *554*, 143–162.
26. Rhein, V.F., Carroll, J., Ding, S., Fearnley, I.M., and Walker, J.E. (2013). NDUFAF7 methylates arginine 85 in the NDUFS2 subunit of human complex I. J. Biol. Chem. *288*, 33016–33026.
27. Rhein, V.F., Carroll, J., He, J., Ding, S., Fearnley, I.M., and Walker, J.E. (2014). Human METTL20 methylates lysine residues adjacent to the recognition loop of the electron transfer flavoprotein in mitochondria. J. Biol. Chem. *289*, 24640–24651.
28. Mourier, A., Motori, E., Brandt, T., Lagouge, M., Atanassov, I., Galinier, A., Rappl, G., Brodesser, S., Hultenby, K., Dieterich, C., and Larsson, N.G. (2015). Mitofusin 2 is required to maintain mitochondrial coenzyme Q levels. J. Cell Biol. *208*, 429–442.
29. Wibom, R., Hagenfeldt, L., and von Döbeln, U. (2002). Measurement of ATP production and respiratory chain enzyme activities in mitochondria isolated from small muscle biopsy samples. Anal. Biochem. *311*, 139–151.
30. Kirby, D.M., Thorburn, D.R., Turnbull, D.M., and Taylor, R.W. (2007). Biochemical assays of respiratory chain complex activity. Methods Cell Biol. *80*, 93–119.
31. Booker, S.J., Cicchillo, R.M., and Grove, T.L. (2007). Self-sacrifice in radical S-adenosylmethionine proteins. Curr. Opin. Chem. Biol. *11*, 543–552.
32. Laredj, L.N., Licitra, F., and Puccio, H.M. (2014). The molecular genetics of coenzyme Q biosynthesis in health and disease. Biochimie *100*, 78–87.

The American Journal of Human Genetics

Supplemental Data

Intra-mitochondrial Methylation Deficiency Due to Mutations in *SLC25A26*

Yoshihito Kishita, Aleksandra Pajak, Nikhita Ajit Bolar, Carlo M.T. Marobbio, Camilla Maffezzini, Daniela V. Miniero, Magnus Monné, Masakazu Kohda, Henrik Stranneheim, Kei Murayama, Karin Naess, Nicole Lesko, Helene Bruhn, Arnaud Mourier, Rolf Wibom, Inger Nennesmo, Ann Jespers, Paul Govaert, Akira Ohtake, Lut Van Laer, Bart L. Loeys, Christoph Freyer, Ferdinando Palmieri, Anna Wredenberg, Yasushi Okazaki, and Anna Wedell

Supplemental Note: case reports

The studies were approved by the regional Ethics Committees at Karolinska Institutet, Sweden, the Saitama Medical University, Japan and Antwerp University Hospital, Belgium. Written informed consent was obtained from the parents.

Individual 1

Individual 1 (P1) was born 2009 in gestational week 39 to consanguineous healthy parents from Iraq. There is one healthy sister born 2006. Pregnancy and neonatal period were normal. Birth weight was 3360 grams, length 53 cm and head circumference 35.5 cm. The boy presented at 4 weeks with acute circulatory collapse and pulmonary hypertension, requiring extra-corporeal membrane oxygenation for 5 days. Urinary organic acid analysis showed increased excretion of lactate, 3-methyl-glutaconic acid and alpha-ketoglutarare but was otherwise normal. There was severe lactic acidosis around 20 mmol/L (ref 0.5-2.3). Sodium dichloroacetic acid had good effect, and the boy slowly normalized. Plasma lactate has since been intermittently slightly elevated but most often within the normal range. Plasma glycine was increased up to 617 μmol/L (ref 80-320) at 5 weeks. Analyses of urinary amino acids, urinary purines and pyrimidines, and plasma acylcarnitines gave normal results.

A lung biopsy performed at 5 weeks showed slight interstitial oedema and muscularized arterioli compatible with pulmonary hypertension of unclear etiology, and discreet presence of hyperplastic pneumocytes and clear cells with increased glycogen, but no signs of capillary alveolar dysplasia, inflammation, or other abnormalities. Computer tomography (CT) of the chest and abdomen showed an enlarged right ventricle of the heart, wide *truncus pulmonalis* and prominent lung artery.

A muscle biopsy was performed at 8 weeks from the *tibialis anterior* muscle. Investigation of isolated muscle mitochondria revealed reduced activities of complex I and IV and reduced ATP production rate. In particular, ATP production was virtually absent using pyruvate as a substrate (Figure S1A and B). Gross muscle histology was unremarkable without any increase in centrally positioned nuclei and no signs of inflammation or increased glycogen content. There was an even ratio of type 1 and type 2 muscle fibres. Combined staining for SDH and COX revealed numerous COX-negative fibres (Figure S1C). There were no ragged red fibres and electron microscopy did not reveal any morphologically abnormal mitochondria. Blue native gel electrophoresis showed reduced amounts of complex I and IV of the respiratory chain (Figure S1D).

Sanger sequencing was performed of the complete mtDNA isolated from muscle and the *PDHA1*, *POLG*, and *TK2* genes from DNA isolated from blood, without positive findings.

At 3.5 years there was a second episode of pulmonary hypertension, which also normalized. An enlarged right atrium and ventricle of the heart was observed by echocardiogram. The boy was treated with sildenafil until 4 years 10 months of age. He has since been cardiopulmonary stable without this treatment.

At 6 years 3 months the boy has increasing muscle weakness, exercise intolerance and fatigue. He walks without support but only short stretches. He has severe problems with recurrent abdominal pain and lack of appetite, and development is slightly delayed.

Individual 2

Individual 2 (P2) was the first child of healthy Japanese parents. There is one healthy younger brother. The girl was born at 39 weeks of gestation. Her birth weight and height were 3076 g (+0.2 SD) and 48.2 cm (-0.7 SD). Apgar scores were 9 at 1 minute and 10 at 5 minutes. Around 11 hours after birth, she developed respiratory failure. Blood lactate was elevated at 41.8 mmol/L (ref <1.8) and showed severe acidosis (pH 6.6). Pyruvate levels were 0.65 mmol/L (ref <0.1). She required mechanical ventilation and peritoneal dialysis. Histology of a muscle biopsy specimen at 6 days indicated no ragged red fibers (RRF) but mild COX deficiencies were observed. There was no mutation in muscle mitochondrial DNA. Blood acylcarnitine analysis showed no abnormality. Urine organic acid analysis also showed no abnormality except for large amount of lactate. Amino acid profiles showed elevated alanine. At 133 days of age, she was discharged from hospital. Resting lactate levels in the blood was persistently high (4.4mmol/L) and acute infections caused an increase in blood lactate (>11.1mmol/L) despite treatment with vitamins, L-carnitine, coenzyme Q and dichloroacetic acid. She could walk at 1 year and her DQ score was 82 at 1 year and 10 months of age. When she was 2 years old, a remarkable hyperlacticacidemia (36.1 mmol/L) was observed, followed by cardiopulmonary arrest and hypoxic brain damage. After this episode she remained severely handicapped. A muscle biopsy was performed at 3 years and showed remarkable ragged RRF and COX deficiencies (Figure S1F). Respiratory chain enzyme activities were normal in fibroblasts but showed decreased complex I, III and IV activities in skeletal muscle (Figure S1E).

Individual 3

Individual 3 (P3), born to consanguineous parents of Moroccan decent, was delivered by caesarean section at 30 weeks 5 days after reduced fetal movements, polyhydramnios, fetal hydrops, and poor cardiotocography (CTG) were noted from 27 weeks of gestational age. She had normal antropometric parameters (birth weight 1300 grams, length 38 cm and head circumference 27.5 cm) but presented with poor Apgar score (3-5-6) due to bradycardia, hypotonia and respiratory insufficiency, necessitating assisted ventilation with high frequency oscillation. She suffered from lactic acidosis (84.6 mmol/L, ref 0.45-2.1 mmol/L) in CSF and urine (18 mmol/mmol creatinine, ref 1-285 μmol/mmol creatinine) and had elevated pyruvate levels (1.2 mmol/mmol

creatinine, ref 1-130 μmol/mmol creatinine) in urine. Brain ultra-sound demonstrated cystic necrosis of germinal matrix (extensive symmetrical caudothalamic germinolysis) and mild striatal arteriopathy. The child died of respiratory and multiple organ failure at 5 days of age. Measurement of respiratory chain activity in fibroblasts demonstrated decreased complex IV activity.

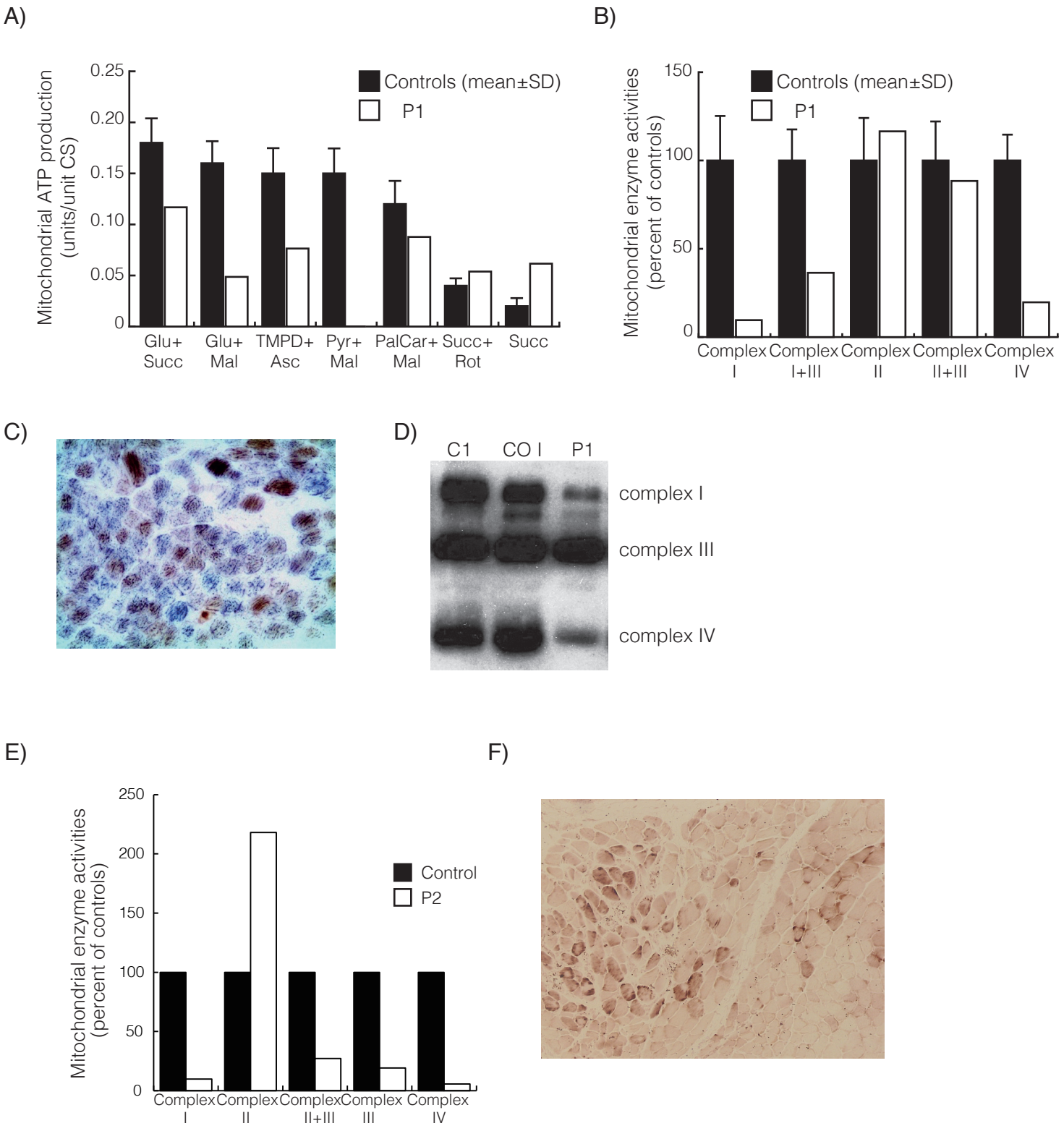

Figure S1: Bioenergetic analyses of mitochondria and muscle histology from individuals P1 and P2. A) Mitochondrial ATP production rate (MAPR) was determined by a firefly luciferase-based method at 25°C, using six different substrate combinations (Glu = glutamate; Succ = succinate; Mal = malate; TMPD = N,N,N',N'-Tetramethyl-p-phenylenediamine dihydrochloride; Asc = ascorbate; Pyr = pyruvate; PalCar = palmitoyl-L-carnitine; Rot = rotenone). Results are presented as the ATP synthesis rate (units) per unit of citrate synthase (CS) activity (control n=11; age 0–5 years). B) Respiratory chain enzyme activities of complex I (NADH:coenzyme Q reductase), complexes I and III (NADH:cytochrome *c* reductase), complex II (succinate dehydrogenase), complexes II and III (succinate:cytochrome *c* reductase, SCR), complex IV (COX) and CS were determined. Results are presented as percentage of mean control (n=9; age 0–5 years) values. The range of control values is depicted as ±SD. (C) cytochrome *c* - succinate dehydrogenase (COX-SDH) double staining of skeletal muscle from P1. (D) Blue-native PAGE followed by Western blot analysis of control (C1), individual with isolated complex I defect (CO I) and P1 skeletal muscle mitochondria. Antibodies against complex I, complex III and complex IV were used. (E) Respiratory chain enzyme activities as in (B) on P2 muscle mitochondria. (F) Cytochrome oxidase (COX) staining of skeletal muscle from 3 years old P2.

A)

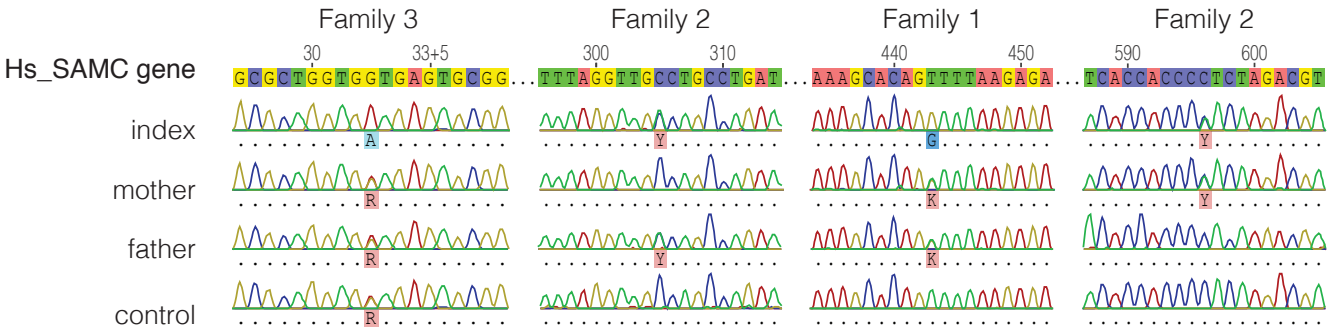

B)

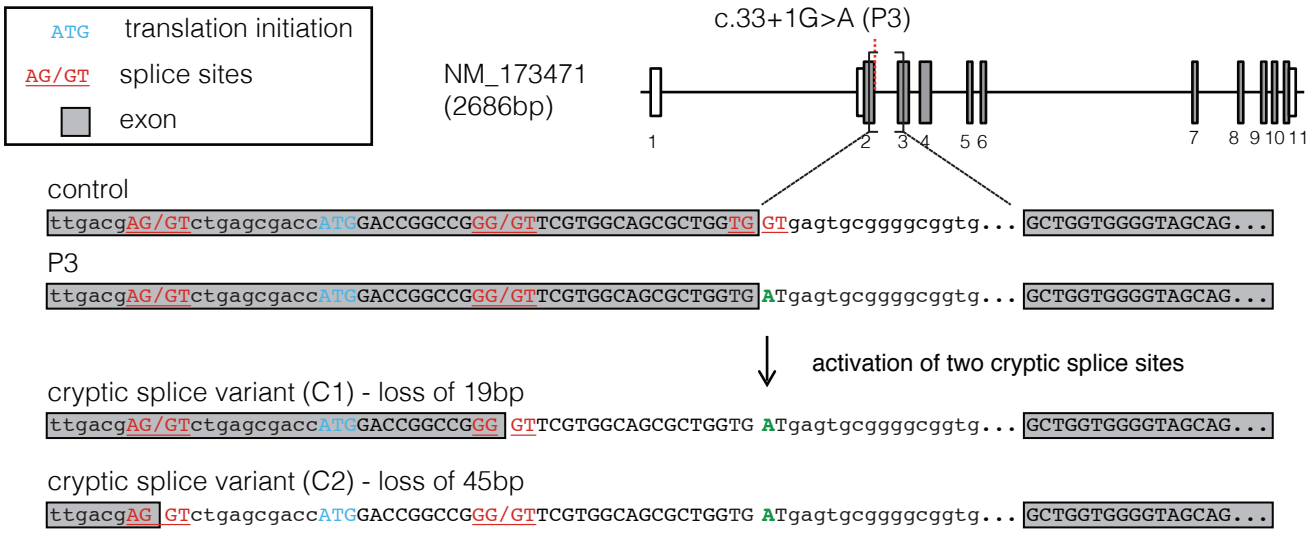

C)

Isoform	splice site used	% of clones indentified (n=48)	
		control	individual P3
P.1	wild type consensus	63.5	0
P.1	cryptic splice site 1 (C1)	0	31.2
P.1	cryptic splice site 2 (C2)	0	54.2
S.1	wild type consensus	36.5	0
S.1	cryptic splice site 1 (C1)	0	0
S.1	cryptic splice site 2 (C2)	0	10.5
S.1	other*	0	4.1

* two other splice isoforms of downstream regions following the UTR of the shorter isoform (S.1) were detected.

Figure S2: Electropherogram from Sanger sequencing results aligned to *SLC25A26*. (A) Fibroblast or blood DNA from family members were used for Sanger sequencing of *SLC25A26* (NM_173471.3). Control sample of family 1 is the unaffected sibling. (B) Schematic diagram showing the cryptic splice variants generated by the c.33+1G>A mutation in P3. (C) Cloning and sequencing of *SLC25A26* splice variants C1 and C2. PCR products from cDNA from control and P3 fibroblasts were cloned into pCRII TOPO vector (Invitrogen) and sequenced to determine the appropriate splice variant. Total number of clones sequenced (n=48).

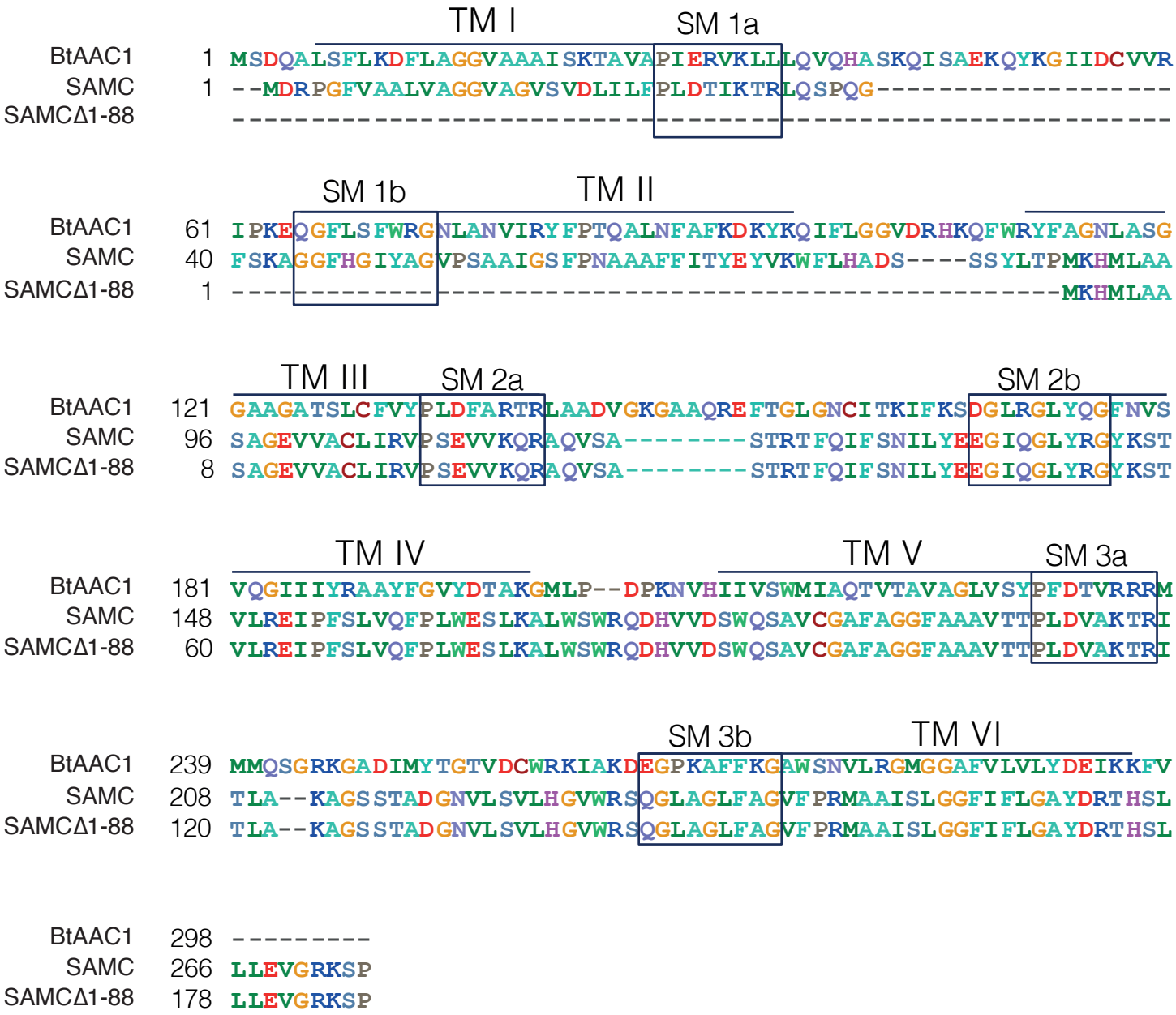

Figure S3. Alignments of the bovine ADP/ATP carrier (BtAAC1), SAMC and SAMCΔ1-88. The six transmembrane a-helices (TM I - TM VI) are linked by hydrophilic segments. The three signature motifs (SM1-SM3) present in the primary structure of the mitochondrial carriers are highlighted.

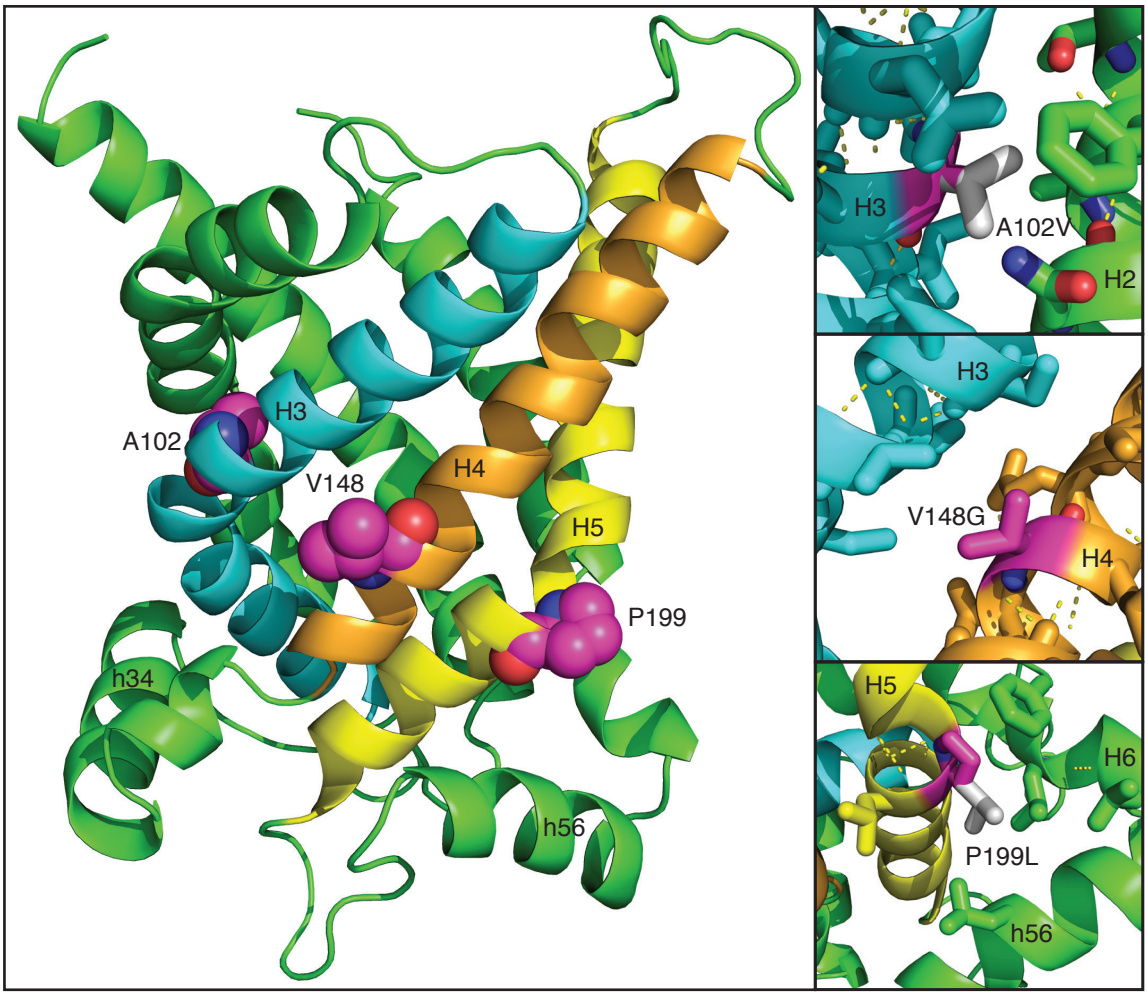

Figure S4: Structural homology model of SAMC illustrating the position of the p.Ala102Val, p.Val148Gly and p.Pro199Leu mutations. The homology model of human SAMC was made with MODELLER by using the carboxyatractyloside-inhibited ADP/ATP carrier structure (PDB ID 1OKC) as a template. The left panel shows the SAMC homology model in cartoon from a lateral view in the membrane plane with transmembrane α-helices H3, H4 and H5 in cyan, orange and yellow, respectively, and the rest of the molecule in green. The mutated residues are shown as spheres in magenta. The right panels show the mutated residues (magenta) and the replacing residues present in the SAMC mutants (white) as sticks at their positions. A102 is located at the interface between transmembrane α-helices H2 and H3. The side chain of V148 protrudes from transmembrane α-helix H4 towards the membrane. P199 creates a kink in transmembrane α-helix H5 in the cytoplasmic conformation of the carrier and its side chain is positioned towards matrix α-helix h56 and transmembrane α-helix H6.

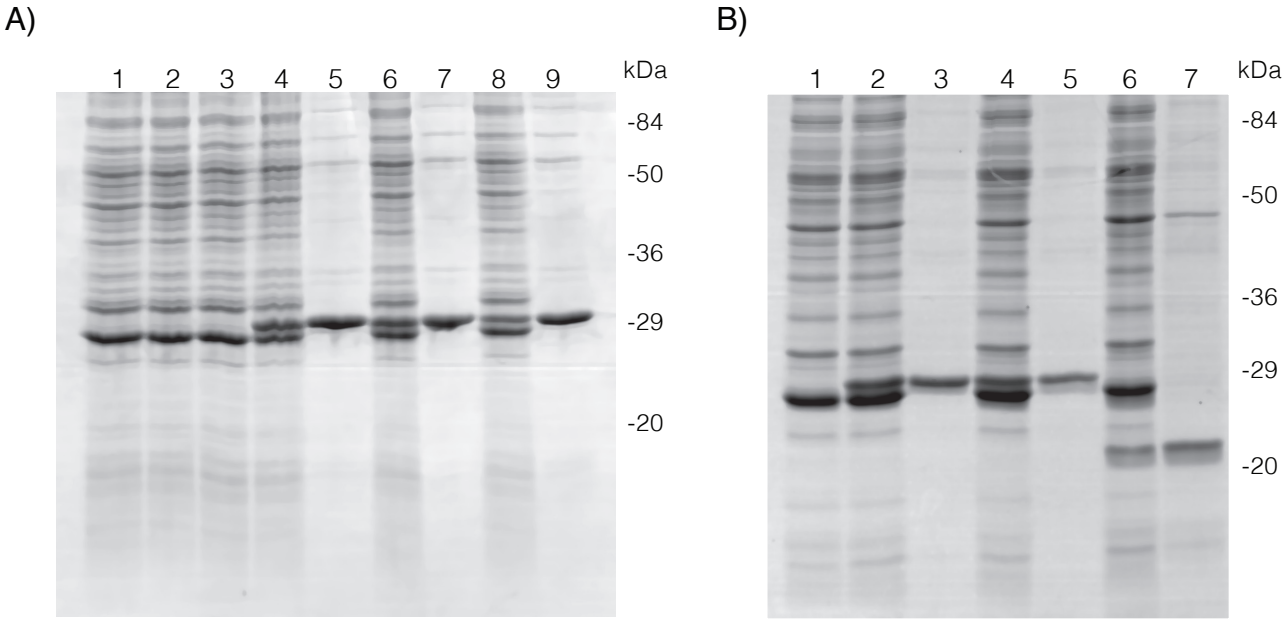

Figure S5. Expression of wild-type and SAMC variants in *E. coli* and their purification. (A) Protein extracts from *E. coli* expresssing control (BL-21 CodonPlus(DE3)-RIL expression vector) (lanes 1,3), wild-type (lanes 2, 4-5), p.Ala102Val (lanes 6-7) and p.Val148Gly (lanes 8-9) SAMC were separated by SDS PAGE and stained with Coomassie Blue. Samples were taken before (lanes 1 and 2) or 5h after (lanes 3, 4, 6 and 8) induction. Lanes 5, 7 and 9 represent purified SAMC (6.2 µg), p.Ala102Val SAMC (4.3 µg) and p.Val148Gly SAMC (4.7 µg) derived from bacteria shown in lanes 4, 6 and 8, respectively. (B) Protein extracts from *E. coli* expresssing control (BL-21 CodonPlus(DE3)-RIL expression vector) (lane 1), wild-type (lanes 2-3), p.Pro199Leu (lanes 4-5) and SAMCΔ1-88 (lanes 6-7) were analyzed as above. Samples were collected 5h after (lanes 1, 2, 4 and 6) induction. Purified samples for SAMC (3.6 µg), p.Pro199Leu SAMC (2.5µg) and SAMCΔ1-88 (3 µg) derived from bacteria shown in lanes 2, 4 and 6 are shown in lanes 3, 5 and 7, respectively.

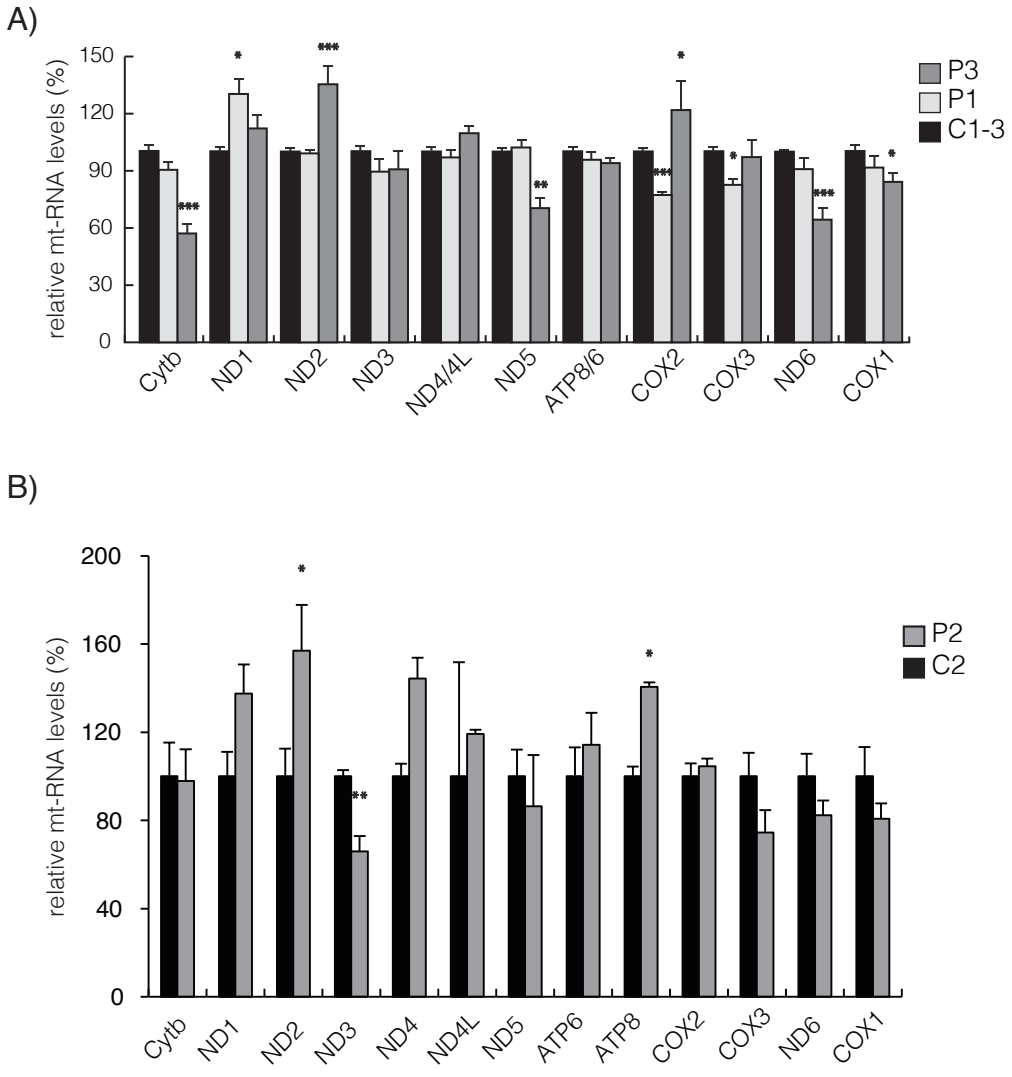

Figure S6: Steady-state levels of the indicated mitochondrial transcripts. Fibroblasts from (**A**) P1 and P3 or (**B**) P2 determined by qRT-PCR. All data are represented as mean ± SEM. (* $p<0.05$, ** $p<0.01$, ***$p<0.001$).